Technical note

Acquisition of full-field strain distributions on ovine fracture callus cross-sections with electronic speckle pattern interferometry

Michael Bottlang[a,*], Marcus Mohr[a], Ulrich Simon[b], Lutz Claes[b]

[a]*Biomechanics Laboratory, Legacy Clinical Research and Technology Center, 1225 NE 2nd Avenue, Portland, OR 97232, USA*
[b]*Institute of Orthopaedic Research and Biomechanics, Ulm, Germany*

Abstract

This study evaluated the feasibility of assessing continuous strain distributions on fracture callus cross-sections with an electronic speckle pattern interferometry (ESPI) system.

Mid-sagittal callus cross-sections were harvested from ovine tibiae. One low stiffness (LS) specimen and one high stiffness (HS) specimen were selected to evaluate the feasibility for strain acquisition over a range of callus properties. The HS specimen was 147 times stiffer in compression than the LS specimen. ESPI captured continuous strain distributions on both specimens. Peak strain was located adjacent to cortical boundaries in the osteotomy gap. In response to 5 N compression, peak compressive strain of 5.8% in the LS specimen was over two orders of magnitude higher than peak compressive strain of 0.013% in the HS specimen.

In conclusion, ESPI-based strain acquisition enables reproducible quantification of strain distributions on callus cross-sections. Such measurements may support validation of computational models and evaluation of experimental results in fracture healing research.
© 2007 Elsevier Ltd. All rights reserved.

Keywords: Fracture; Healing; Callus; Strain

1. Introduction

The effects of interfragmentary strain on fracture callus formation have been studied with experimental and theoretical models. However, the lack of methods for direct strain measurements in a fracture callus hinders evaluation of experimental results and validation of theoretical models.

Experimental *in vivo* studies typically estimated strain in fracture callus based on interfragmentary motion relative to the fracture gap size (Augat et al., 1996; Claes et al., 1998; Goodship et al., 1998). Consequently, strain estimates are limited to the assumption of a homogeneous strain distribution in the fracture gap. Computational models can estimate strain and pressure distributions as well as fluid flow in the fracture callus (Carter et al., 1998; Claes and Heigele, 1999; Cheal et al., 1991; Gomez-Benito et al., 2005; Isaksson et al., 2006; Lacroix and Prendergast,

2002). However, the accuracy of these theoretical models is limited to the extent of their physical validation.

The present study evaluated the feasibility and reproducibility of strain distribution assessment on fracture callus cross-sections with electronic speckle pattern interferometry (ESPI).

2. Method

2.1. Specimens

Mid-sagittal callus cross-sections of 3 mm thickness were obtained from four sheep following tibial osteotomy treated by 8 weeks of external fixation. One specimen with low stiffness (LS) and one specimen with high stiffness (HS) in compression were selected to evaluate the feasibility for ESPI strain acquisition over a range of callus properties. Specimens were submersed in physiologic saline and kept frozen at $-18\,^\circ$C until testing.

2.2. Experimental setup

Specimens were mounted in a uni-axial loading stage for application of unconfined compression and tension (Fig. 1a). Load was applied manually

---

*Corresponding author. Tel.: +1 503 413 5457; fax: +1 503 413 5216.
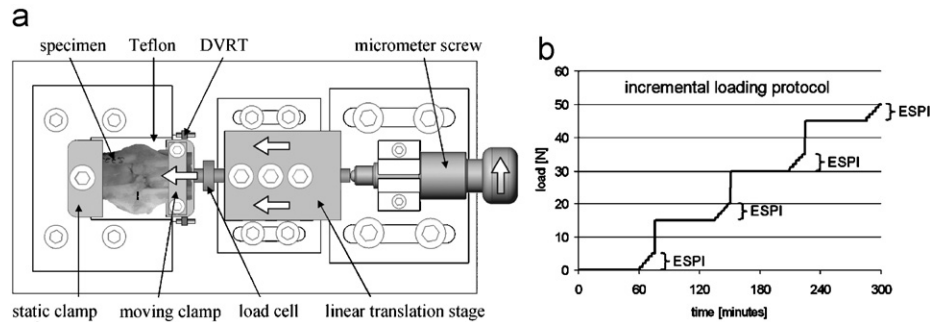E-mail address: mbottlang@biomechresearch.org (M. Bottlang).

Fig. 1. (a) Experimental setup for loading of callus specimens in unconfined axial compression. A Teflon® insert on the loading stage minimized friction between the specimen and its support surface. The specimen chamber was sealed from airflow to minimize specimen drying. (b) Incremental loading protocol for ESPI analysis.

using a micrometer screw and a translation stage (M-461/DS-4F, Newport Co., Irvine, CA). Clamp-to-clamp displacement was measured by displacement sensors (M-DVRT-3-SK4, Microstrain, Burlington, VT) with 1.5 μm resolution. Axial load was measured with a ±500 N load cell (ELFS-T4M, Entran, Fairfield, NJ). Real-time averaging of the load cell signal in Labview® software provided 0.2 N resolution.

2.3. Stiffness measurement

Specimens were pre-conditioned by application of three tension and compression cycles up to 30 N, followed by 1-h equilibration of the unloaded specimen. Pre-conditioning was applied to support reproducible measurement conditions. Compressive and tensile stiffness was measured in response to 5 N loading.

2.4. ESPI strain acquisition

The sensor of an ESPI system (Q100, Ettemeyer AG, Nersingen, Germany) was suspended over the callus specimen. It measured surface displacement in three directions at 512×512 locations over a 37 mm × 28 mm region of interest (ROI). To optimize reflective properties, a thin layer of titanium dioxide powder (ProCAD, Ivoclar AG, Schaan, Liechtenstein) was dispersed on the specimen surface (Erne et al., 2005). The ESPI system captured displacement at a resolution of less than 1/10 of the laser wavelength ($\lambda = 680$ nm). Due to this high sensitivity, individual ESPI measurements were limited to small incremental loading steps. To capture larger deformations, sequential ESPI recordings were acquired and cumulatively evaluated. Strain was calculated based on a 72 μm gage length after smoothing over a 216 μm array width.

Strain distributions were acquired under compression and tension. First, compression was applied at pre-loads of 0, 15, 30, and 45 N (Fig. 1b). At each pre-load, specimens were equilibrated for 1 h. Subsequently, a series of incremental compression steps was applied for ESPI analysis. Incremental load steps were adjusted to yield an interference fringe density with distinctly visible fringes that could be individually resolved by the system software. Therefore, the magnitude of incremental load steps at each pre-load depended on the specimen stiffness. Incremental load steps were applied up to a cumulative load of 5 N. In cases were the last load step did not exactly result in a 5 N cumulative load, strain results were normalized to a 5 N cumulative load. Strain maps were expressed in terms of minimal principal strain ε_C. The same loading protocol was repeated in tension to acquire maps of maximal principal strain ε_T.

Reproducibility of ESPI measurements was assessed by re-mounting and testing the HS specimen three times in compression at 30 N pre-load. Additionally, out-of-plane deformation at 30 N pre-load was obtained from ESPI reports for both specimens to complement in-plane strain results.

Finally, contact radiographs of both specimens were obtained. The outline of cortices were digitized on these contact radiographs and superimposed on strain maps to aid visualization of distinct callus regions.

3. Results

The HS specimen had a compressive stiffness of 10.3 kN/mm and was 147 times stiffer than the LS specimen (0.07 kN/mm). The tensile stiffness of the HS and LS specimen was 13.2 and 0.42 kN/mm, respectively.

ESPI delivered continuous strain maps on both callus cross-sections, with the exception of the medullary canals that contained structurally unstable soft tissue.

On the HS specimen, the highest strain was detected adjacent to cortical boundaries in the osteotomy gap under compression and tension (Fig. 2). Peak ε_C under 5 N compression at 0, 15, 30, and 45 N pre-load was 0.013%, 0.011%, 0.013%, and 0.013%, respectively. Under 5 N tension at 0, 15, 30, and 45 N tensile pre-load, peak ε_T was 0.007%, 0.009%, 0.010%, and 0.009%, respectively. Strain distributions and strain magnitudes were highly reproducible, yielding a standard deviation of 9.1% of the average peak strain (Fig. 3).

The peak strain in the LS specimen was determined to be 80% lower in tension than in compression (Fig. 4). Peak ε_C under 5 N compression at 0, 15, 30, and 45 N pre-load was 0.730%, 3.428%, 5.791%, and 2.093%, respectively. Under 5 N tension at 0, 15, 30, and 45 N tensile pre-load, peak ε_T was 0.684%, 2.452%, 1.003%, and 0.490%, respectively.

Out-of-plane displacement under 5 N tension or compression at 30 N pre-load remained below 1 μm for the HS specimen (Fig. 5a), and ranged from −52 to 31 μm (compression) and −16 to 2.3 μm (tension) for the LS specimen (Fig. 5b).

4. Discussion

Speckle pattern interferometry has been used since 1987 in a semi-quantitative manner (Katz et al., 1998; Manley et al., 1987; Ovryn et al., 1987). More recently, ESPI has been advanced into a quantitative strain measurement technology, and has been applied on the femoral cortex
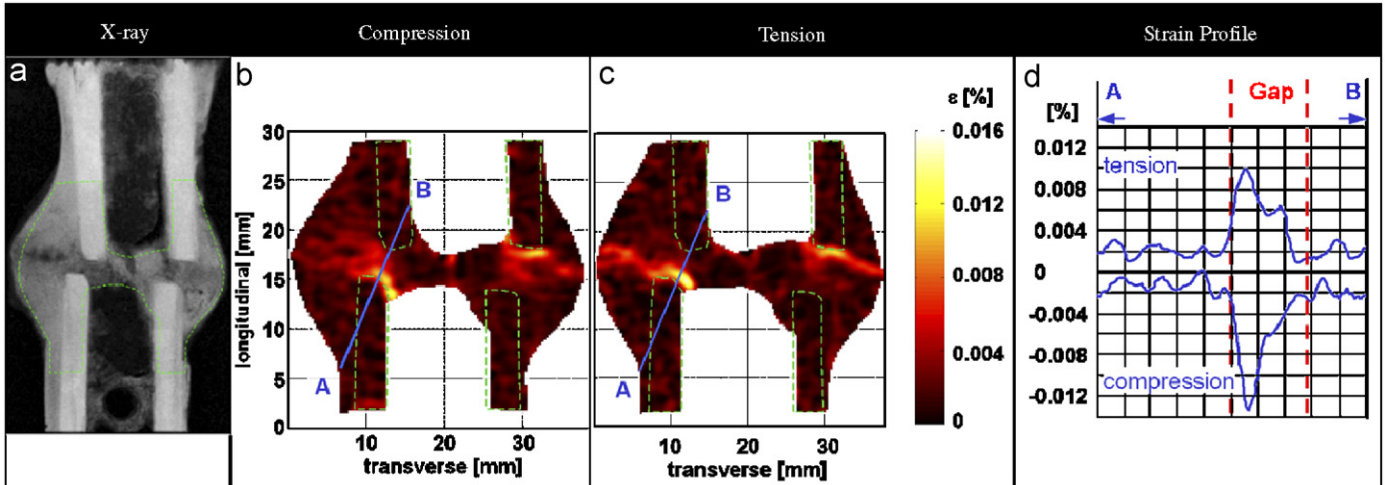
Fig. 2. HS specimen: (a) contact radiograph, depicting the ESPI evaluation region; (b) compressive strain, depicted in absolute values of ε_C; and (c) tensile strain in response to 5 N loading at 30 N pre-load, shown with cortex boundaries extracted from contact radiographs; (d) compressive and tensile strain profiles along line A–B across the osteotomy gap.
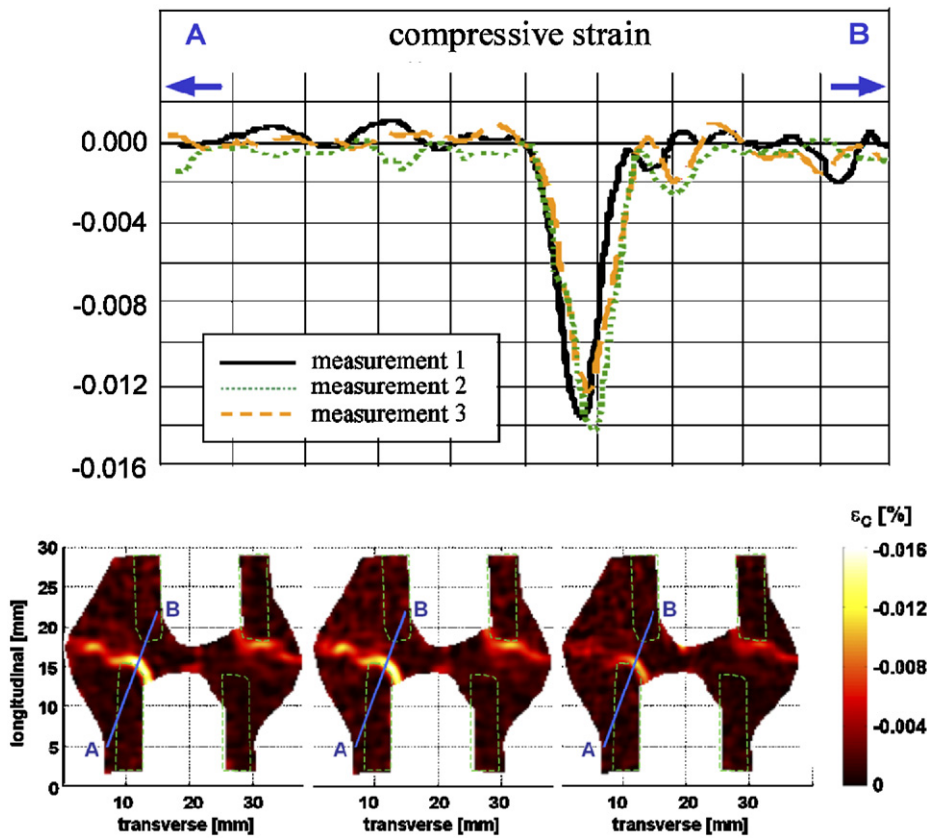

Fig. 3. Three reproducibility measurements on the HS specimen under 5 N compression at 30 N pre-load.

(Kirkpatrick and Brooks, 1998), on cortical bone cubes (Shahar et al., 2007), and on tooth enamel (Lang et al., 2004). The ESPI system of this study has previously been applied on bone (Bottlang et al., 2006) and cartilage (Erne et al., 2005). In the present study, ESPI captured strain on specimens with highly non-uniform material properties, ranging from soft tissue to cortical bone. For this purpose,

ESPI demonstrated three benefits: its high sensitivity enabled measurement of strain smaller than 0.01%. Its high spatial resolution enabled extraction of strain gradients in the fracture gap. Finally, its ROI encompassed the entire callus cross-section. Therefore, ESPI can achieve a higher sensitivity and resolution for a given ROI than marker-based image correlation techniques (Guilak et al.,
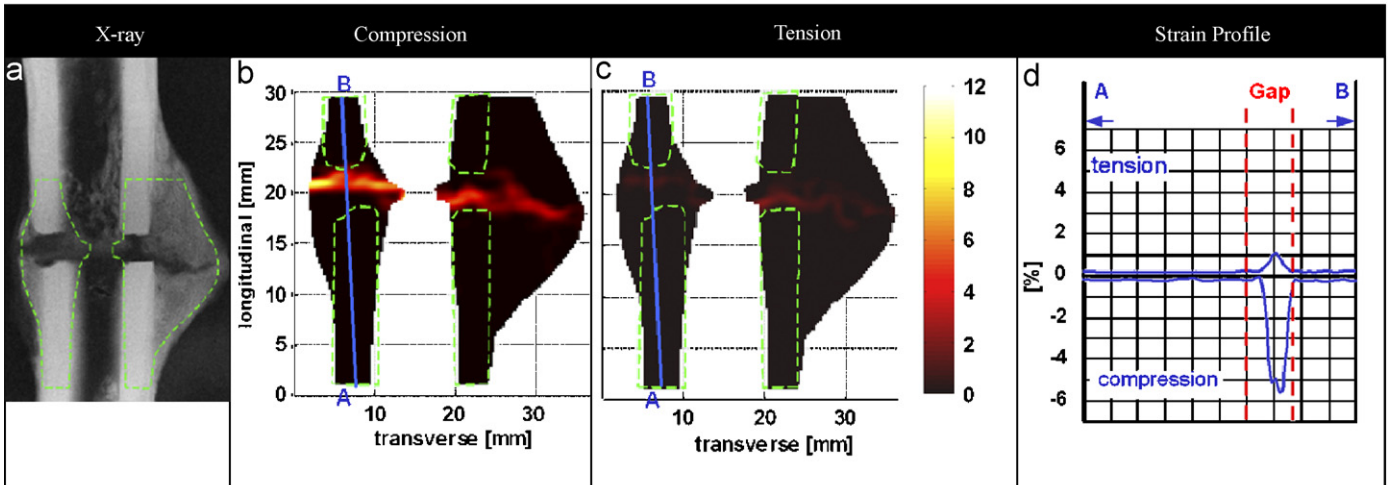
Fig. 4. LS specimen: (a) contact radiograph; (b) compressive strain, depicted in absolute values of ε_C; and (c) tensile strain in response to 5 N loading at 30 N pre-load; (d) compressive and tensile strain profiles along line A–B across the osteotomy gap.
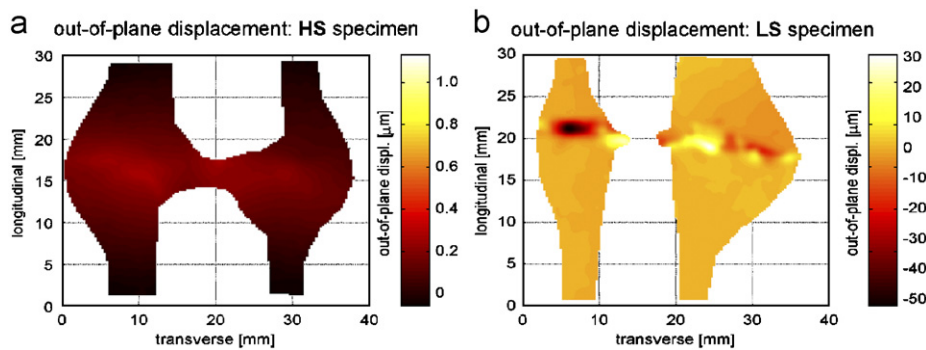

Fig. 5. Out-of plane displacement in response to 5 N compression at 30 N pre-load shown for the HS specimen (a), and LS specimen (b).

1995; Schinagl et al., 1996; Wang et al., 2003; Thompson et al., 2007).

ESPI exhibits several limitations. Its high sensitivity required incremental loading in a quasi-static manner. Therefore, the present results are not readily comparable to absolute strain thresholds proposed in theoretical models of fracture healing. Furthermore, ESPI requires optical access to the measurement surface for which reason callus cross-sections have been evaluated. Unlike in the intact callus, the callus cross-section is not constrained by surrounding tissue. Therefore, out-of-plane displacement has been reported in addition to in-plane strain. While the reported strain distributions cannot be readily compared to computational results of a complete fracture callus, the well-defined specimen geometry and loading condition of the cross-sectional specimen is advantageous for simulation in a simplified computational model. Such a model, upon validation based on experimental results, can be extrapolated into a complete callus model. Finally, specimens underwent one freezing and thawing cycle, which may have affected mechanical properties.

In conclusion, results of this study support the value of ESPI to generate reproducible, quantitative, and conti-nuous strain maps on fracture callus cross-sections. These experimentally derived strain results may serve to validate computational models and to evaluate callus specimens in experimental studies of fracture healing.

Conflict of interest

None of the authors have any potential conflict of interest regarding the article.

References

Augat, P., Merk, J., Ignatius, A., Margevicius, K., Bauer, G., Rosenbaum, D., et al., 1996. Early, full weightbearing with flexible fixation delays fracture healing. Clinical Orthopaedics and Related Research, 194–202.

Bottlang, M., Erne, O.K., Lacatusu, E., Sommers, M.B., Kessler, O., 2006. A mobile-bearing knee prosthesis can reduce strain at the proximal tibia. Clinical Orthopaedics and Related Research 447, 105–111.

Carter, D.R., Beaupre, G.S., Giori, N.J., Helms, J.A., 1998. Mechan-obiology of skeletal regeneration. Clinical Orthopaedics and Related Research, S41–S55.

Cheal, E.J., Mansmann, K.A., DiGioia III, A.M., Hayes, W.C., Perren, S.M., 1991. Role of interfragmentary strain in fracture healing: ovine

model of a healing osteotomy. Journal of Orthopaedic Research 9, 131–142.

Claes, L.E., Heigele, C.A., 1999. Magnitudes of local stress and strain along bony surfaces predict the course and type of fracture healing. Journal of Biomechanics 32, 255–266.

Claes, L.E., Heigele, C.A., Neidlinger-Wilke, C., Kaspar, D., Seidl, W., Margevicius, K.J., et al., 1998. Effects of mechanical factors on the fracture healing process. Clinical Orthopaedics and Related Research, S132–S147.

Erne, O.K., Reid, J.B., Ehmke, L.W., Sommers, M.B., Madey, S.M., Bottlang, M., 2005. Depth-dependent strain of patellofemoral articular cartilage in unconfined compression. Journal of Biomechanics 38, 667–672.

Gomez-Benito, M.J., Garcia-Aznar, J.M., Kuiper, J.H., Doblare, M., 2005. Influence of fracture gap size on the pattern of long bone healing: a computational study. Journal of Theoretical Biology 235 (1), 105–119.

Goodship, A.E., Cunningham, J.L., Kenwright, J., 1998. Strain rate and timing of stimulation in mechanical modulation of fracture healing. Clinical Orthopaedics and Related Research, S105–S115.

Guilak, F., Ratcliffe, A., Mow, V.C., 1995. Chondrocyte deformation and local tissue strain in articular cartilage: a confocal microscopy study. Journal of Orthopaedic Research 13, 410–421.

Isaksson, H., Wilson, W., van Donkelaar, C.C., Huiskes, R., Ito, K., 2006. Comparison of biophysical stimuli for mechano-regulation of tissue differentiation during fracture healing. Journal of Biomechanics 39, 1507–1516.

Katz, D.M., Blatcher, S., Shelton, J.C., 1998. Quantification of holographic fringe data: comparison of intact and implanted femurs. Medical Engineering & Physics 20, 114–123.

Kirkpatrick, S.J., Brooks, B.W., 1998. Micromechanical behavior of cortical bone as inferred from laser speckle data. Journal of Biomedical Materials Research 39 (3), 373–379.

Lacroix, D., Prendergast, P.J., 2002. A mechano-regulation model for tissue differentiation during fracture healing: analysis of gap size and loading. Journal of Biomechanics 35, 1163–1171.

Lang, H., Rampado, M., Mullejans, R., Raab, W.H., 2004. Determination of the dynamics of restored teeth by 3D electronic speckle pattern interferometry. Lasers in Surgery and Medicine 34, 300–309.

Manley, M.T., Ovryn, B., Stern, L.S., 1987. Evaluation of double-exposure holographic interferometry for biomechanical measurements in vitro. Journal of Orthopaedic Research 5, 144–149.

Ovryn, B., Manley, M.T., Stern, L.S., 1987. Holographic interferometry: a critique of the technique and its potential for biomedical measurements. Annals of Biomedical Engineering 15, 67–78.

Schinagl, R.M., Ting, M.K., Price, J.H., Sah, R.L., 1996. Video microscopy to quantitate the inhomogeneous equilibrium strain within articular cartilage during confined compression. Annals of Biomedical Engineering 24, 500–512.

Shahar, R., Zaslansky, P., Barak, M., Friesem, A.A., Currey, J.D., Weiner, S., 2007. Anisotropic Poisson's ratio and compression modulus of cortical bone determined by speckle interferometry. Journal of Biomechanics 40 (2), 252–264.

Thompson, M.S., Schell, H., Lienau, J., Duda, G.N., 2007. Digital image correlation: a technique for determining local mechanical conditions within early bone callus. Medical Engineering & Physics 29 (7), 820–823.

Wang, C.C., Chahine, N.O., Hung, C.T., Ateshian, G.A., 2003. Optical determination of anisotropic material properties of bovine articular cartilage in compression. Journal of Biomechanics 36, 339–353.